Thermo-piezo-elastic analysis of amplified piezoceramic actuators using a refined one-dimensional model

Thermo-piezo-elastic Analysis of Amplified Piezo-ceramic Actuators Using a Refined One-dimensional Model

Journal Title
XX(X):1–11

DOI: 10.1177/ToBeAssigned
www.sagepub.com/
SAGE

Enrico Zappino[1] and Erasmo Carrera[2]

Abstract

The thermo-piezo-elastic analysis of amplified piezo-ceramic actuators is presented in this paper. A refined one-dimensional multi-field finite element (FE) model, based on the Carrera Unified Formulation, has been developed. Thermal and piezoelectric effects have been included in the structural model and a fully-coupled thermo-piezo-elastic analysis has been performed. The FE model has been assessed by comparing it with results from open literature The model has also been used to perform the analysis of complex amplified piezoceramic actuators. These actuators are able to amplify the displacements produced by piezoceramic material but, they suffer from high deformations when they undergo to high thermal loads. An accurate thermal analysis has been performed to evaluate the strain/stress field. The results show the accuracy of the present model and its capabilities in multi-field analyses.

Keywords

One-dimensional models, Carrera Unified Formulation, Thermo-piezo-elastic analysis, Multi-field analysis.

Introduction

The use of advanced materials for the design of high-performances actuators may lead to a step forward in the performances of next-generation aircraft engines. AeroPZT European project, funded in the framework of the Clean-sky project, has the aim of investigating the possibility of using piezoelectric materials for the design of high-performance actuators that are able to operate at high temperature and in harsh conditions.

The piezoelectric effect has been known since the 19^{th} century when the Curie brothers first noticed it. It consists of the conversion of mechanical to electrical energy and vice-versa. The use of such materials in structural design is very attractive because of their properties, and a great deal of efforts has been made to include the piezoelectric contribution in structural models. Crawley and Luis (1987) and Bailey and Hubbard (1985) considered the piezoelectric contribution as an additional strain which had to be added to the inactive structure. Classical structural models were widely used to analyze piezoelectric materials; as shown by Sarvanos and Heyliger (1999) in their review. In the past, classical three-dimensional (Dong et al. (2006); Xu and Koko (2004)), two-dimensional (Kim and Kim (2005); Moitha et al. (2004)) and one-dimensional models were used to study structures with piezoelectric effects. The use of refined structural models improves the accuracy of the stress and strain fields, especially when complex structures, such as multi-layered structures, are considered. A great deal of effort has been focused on the extension of these models to the analysis of piezoelectric materials. One of the most critical points is the interface between the structure and piezoelectric patches, as shown by Zhou and Tiersten (1994). The introduction of shear effects, see Caruso et al. (2003); Kumar and Narayanan (2007); Kusculuoglu and Royston (2005); Liu et al. (2004); Vasques and Rodrigues (2006), make it possible to have a more accurate description of the stress field of the problem. More refined approaches have been proposed in the last few years, see Zhou et al. (2000); Moita et al. (2005); Vidal et al. (2011); in these cases, a first order theory has been considered. Carrera (1997), Robaldo et al. (2006) and Carrera et al. (2007) proposed the use of refined two-dimensional models for the analysis of multi-layered structures, including piezoelectric materials. Biscani et al. (2012) proposed an approach that is able to increase the accuracy of the model but only where piezoelectric elements are located. These materials can be used in the development of high-performance actuators but, when a high stroke is needed, an amplification device, usually metallic, is required. The coupling between piezo-ceramic and metallic materials can be an issue when the device has to operate at high temperatures. The large difference between the thermal expansion coefficients (CTE) could lead to large deformations, which could overcome the stroke of the actuator. The use of accurate numerical models may predict the behavior of these devices and they can be used in the design process. The use of classical beam models for the thermo-piezo-elastic analysis of multilayer structures can be found in the work by Tzou and Ye (1994) and Ahmad et al. (2006). Carrera and Robaldo (2007) presented a class of refined two-dimensional models for the accurate analysis of plates and shells including thermal and piezoelectric effects.

[1]Research fellow, Politecnico di Torino, Turin, Italy
[2]Full Professor, Politecnico di Torino, Turin, Italy

Corresponding author:
Enrico Zappino, Politecnico di Torino Corso Duca degli Abruzzi, 24,10029 Torino, Italy.
Email: enrico.zappino@polito.it

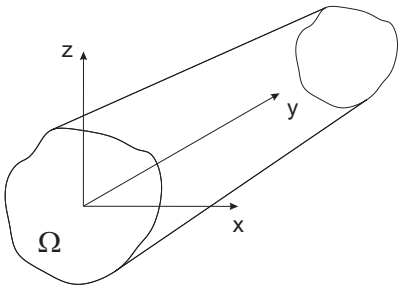

Figure 1. Beam reference system.

The present work has the aim of performing an accurate thermo-piezo-elastic analysis of piezoelectric actuators using a refined one-dimensional model. The activities have been carried out in the frameworks of the AeroPZT project. The actuator was designed by CEDRAT and PI, while, NOLIAC was in charge of the material development. The structural model, developed by the Politecnico di Torino (POLITO), is based on the Carrera Unified Formulation (CUF). The CUF was firstly developed for two-dimensional models by Carrera (2003) and was extended to the thermal-elastic problem by Carrera (2000) and Robaldo et al. (2005). The piezo-elastic formulation was introduced by Robaldo et al. (2006). The fully coupled piezo-thermo-mechanical expansion of the CUF was presented by Carrera and Boscolo (2007). This numerical approach was extended to the one-dimensional model by Carrera et al. (2010, 2011b, 2012a,b),more details can be found in the books by Carrera et al. (2014, 2011a). In the work by Carrera and Petrolo (2012), the displacement field above the cross-section was described using Lagrange-type polynomials. The extension of this model to an analysis of the multi-field analysis was presented by Miglioretti et al. (2014) for the piezo-mechanical problem, and used by Zappino et al. (2016). The present paper introduce for the first time a coupled thermo-piezo-elastic one-dimensional formulation based on the CUF. The model has been assessed and the results have been compared with those present in literature. The present model has been used to perform the analysis of two different amplified piezoelectric actuators. The static response of the devices and the impact of the thermal loads on the mechanical performances have been investigated.

Thermo-piezo-elastic one-dimensional model

This section presents the refined one-dimensional model used in the following analyses. The coordinate reference frame is shown in Fig. 1. The displacement three-dimensional field is described using the vector $\boldsymbol{u}$:

$$\boldsymbol{u}^T = \{u_x,\ u_y,\ u_z\} \tag{1}$$

In the thermo-piezo-elastic formulation, in addition to the mechanical variables, also the temperature variation,ϑ, and the electric potential, ϕ, must be considered. The solution of the thermo-piezo-elastic problem requires to define five quantities in each point:

$$\boldsymbol{q}^T = \{u_x,\ u_y,\ u_z,\ \vartheta,\ \phi\} \tag{2}$$

where vector $\boldsymbol{q}$ contains the unknown quantities.

Kinematic approximation

The one-dimensional approximation requires to assume a known displacement field, a temperature variation and a electric potential over the cross-section. The unknowns vector $\boldsymbol{q}$ can be written as:

$$\mathbf{q} = \mathbf{q}_\tau(y) F_\tau(x,z), \qquad \tau = 1 \dots M. \tag{3}$$

Where the function $F_\tau(x,z)$ is the functions expansion over the cross-section and $\mathbf{q}_\tau(y)$ is the unknown vector along the beam axis. M is the number of terms in the functions expansion $F_\tau(x,z)$. The displacements field, the temperature variation and the electric potential are described using the same formulation. The choice of the functions expansion allows the kinematic of the model to be modified. The Lagrange polynomials are herein used to describe the cross-section unknowns. Nine-point, L9, polynomials are adopted. In the case of an L9 element, the interpolation functions are given by

$$\begin{aligned} F_\tau =& \frac{1}{4}(r^2 + r r_\tau)(s^2 + s s_\tau) \qquad \tau = 1,3,5,7 \\ F_\tau =& \frac{1}{2} s_\tau^2 (s^2 + s s_\tau)(1 - r^2) + \\ & \frac{1}{2} r_\tau^2 (r^2 + r r_\tau)(1 - s^2) \qquad \tau = 2,4,6,8 \\ F_\tau =& (1 - r^2)(1 - s^2) \qquad \tau = 9 \end{aligned} \tag{4}$$

where r and s vary from 1 to +1.

The finite element method approximates the axial unknowns $\mathbf{q}_\tau(y)$ using the one-dimensional shape functions N_i, that is, the unknowns vector assumes the formulation:

$$\mathbf{q} = \mathbf{q}_{i\tau} N_i(y) F_\tau(x,z), \quad \tau = 1 \dots M; \quad i = 1 \dots N_n. \tag{5}$$

Where N_i are the shape functions introduced by the FE model and N_n is the number of nodes of the element. $\mathbf{q}_{i\tau}$ are the nodal unknowns.

Geometrical relations

The geometrical relations in the case of the thermo-piezo-elastic model allow the strain ($\boldsymbol{\varepsilon}$), the spatial thermal variations ($\boldsymbol{\theta}$) and the electric field ($\boldsymbol{E}$) to be evaluated. The strain vector, $\boldsymbol{\varepsilon}$, can be written as:

$$\boldsymbol{\varepsilon}^T = \{\varepsilon_{xx}\ \varepsilon_{yy}\ \varepsilon_{zz}\ \varepsilon_{xz}\ \varepsilon_{yz}\ \varepsilon_{xy}\} = \boldsymbol{D}_u \boldsymbol{u} \tag{6}$$

where $\boldsymbol{D}_u$ is:

$$\boldsymbol{D}_u^T = \begin{bmatrix} 0 & 0 & \partial_z & \partial_x & \partial_y & 0 \\ 0 & \partial_y & 0 & 0 & \partial_z & \partial_x \\ \partial_x & 0 & 0 & \partial_z & 0 & \partial_y \end{bmatrix} \tag{7}$$

The spatial temperature variation, $\boldsymbol{\theta}$, can be written as:

$$\boldsymbol{\theta}^T = \{\vartheta_x\ \vartheta_y\ \vartheta_z\} = \boldsymbol{D}_\vartheta \vartheta \tag{8}$$

where $\boldsymbol{D}_\vartheta$ is:

$$\boldsymbol{D}_\vartheta^T = \begin{bmatrix} \partial_x & \partial_y & \partial_z \end{bmatrix} \tag{9}$$

The electric field, $\boldsymbol{E}$, can be expressed as:

$$\boldsymbol{E}^T = \{\phi_x\ \phi_y\ \phi_z\} = \boldsymbol{D}_\phi \phi \tag{10}$$

where $\boldsymbol{D}_\phi$ is equal to $\boldsymbol{D}_\vartheta$. The symbol ∂ thants for partial derivative, that is: $\partial_x = \frac{\partial}{\partial x}$, $\partial_y = \frac{\partial}{\partial y}$ and $\partial_z = \frac{\partial}{\partial z}$

Constitutive relations

The constitutive equation for the thermo-piezo-elastic model have been derived in according with the work presented by Carrera et al. (2008).

The stress, $\boldsymbol{\sigma}$ can be written in the following form:

$$\boldsymbol{\sigma} = \boldsymbol{C}\boldsymbol{\varepsilon} - \boldsymbol{\lambda}\vartheta - \boldsymbol{e}\boldsymbol{E} \tag{11}$$

The first contribution come from the Hook's law and derives from the mechanical problem.

$$\begin{Bmatrix} \sigma_{xx} \\ \sigma_{yy} \\ \sigma_{zz} \\ \sigma_{xz} \\ \sigma_{yz} \\ \sigma_{xy} \end{Bmatrix} = \begin{bmatrix} C_{11} & C_{12} & C_{13} & 0 & 0 & C_{16} \\ C_{21} & C_{22} & C_{23} & 0 & 0 & C_{26} \\ C_{31} & C_{32} & C_{33} & 0 & 0 & C_{36} \\ 0 & 0 & 0 & C_{44} & C_{45} & 0 \\ 0 & 0 & 0 & C_{54} & C_{55} & 0 \\ C_{61} & C_{62} & C_{63} & 0 & 0 & C_{66} \end{bmatrix} \begin{Bmatrix} \epsilon_{xx} \\ \epsilon_{yy} \\ \epsilon_{zz} \\ \epsilon_{xz} \\ \epsilon_{yz} \\ \epsilon_{xy} \end{Bmatrix} \tag{12}$$

The second therm, $\boldsymbol{\lambda}\vartheta$, comes from the thermo-mechanical coupling. The vector $\boldsymbol{\lambda}$ can be written as:

$$\boldsymbol{\lambda} = \boldsymbol{C}\boldsymbol{\alpha} = \boldsymbol{C}\{\alpha_1 \ \alpha_2 \ \alpha_3 \ 0 \ 0 \ 0 \ \}^T \tag{13}$$

Where $\boldsymbol{C}$ is the matrix with the elastic coefficients of the material, and $\boldsymbol{\alpha}$ is the vector of the thermal expansion coefficients. The last term, $\boldsymbol{e}\boldsymbol{E}$, comes from the electro-mechanical coupling. The matrix $\boldsymbol{e}$ contains the piezoelectric stiffness coefficients and can be written as:

$$\boldsymbol{e} = \boldsymbol{C}\boldsymbol{d} = \boldsymbol{C} \begin{bmatrix} 0 & 0 & 0 & 0 & d_{15} & 0 \\ 0 & 0 & 0 & d_{24} & 0 & 0 \\ d_{31} & d_{32} & d_{33} & 0 & 0 & 0 \end{bmatrix}^T \tag{14}$$

where $\boldsymbol{d}$ is the matrix of the piezoelectric coefficients.

The electric displacement, $\boldsymbol{D}$, can be written in the following form:

$$\boldsymbol{D} = \boldsymbol{e}\boldsymbol{\varepsilon} + \boldsymbol{\chi}\boldsymbol{E} + \boldsymbol{p}\vartheta \tag{15}$$

The first term, $\boldsymbol{e}\boldsymbol{\varepsilon}$, comes from the electro-mechanical coupling. The second contribution, $\boldsymbol{\chi}\boldsymbol{E}$, is due to the electric problem, $\boldsymbol{\chi}$ is to the dielectric permittivity matrix of the material:

$$\boldsymbol{\chi} = \begin{bmatrix} \chi_{11} & \chi_{12} & 0 \\ \chi_{21} & \chi_{22} & 0 \\ 0 & 0 & \chi_{33} \end{bmatrix} \tag{16}$$

The last term, $\boldsymbol{p}\vartheta$, comes from the thermo-electric problem and $\boldsymbol{p}$ is the vector of the pyro-electric coefficients.

The last constitutive equation describe the heat flux, $\boldsymbol{h}$:

$$\boldsymbol{h} = \boldsymbol{\kappa}\boldsymbol{\theta} \tag{17}$$

where $\boldsymbol{\kappa}$ is the conductivity coefficients matrix:

$$\boldsymbol{\kappa} = \begin{bmatrix} \kappa_{11} & \kappa_{12} & 0 \\ \kappa_{21} & \kappa_{22} & 0 \\ 0 & 0 & \kappa_{33} \end{bmatrix} \tag{18}$$

Governing equation

The governing equation can be written using the virtual displacements principle, PVD:

$$\delta L_{int} = \delta L_{ext} \tag{19}$$

where δL_{int} is the virtual variation of the internal work while, δL_{ext} is the virtual variation of the external work.

In explicit form the PVD can be written as:

$$\delta L_{int} = \int_V (\delta\boldsymbol{\varepsilon}^T\boldsymbol{\sigma} - \delta\boldsymbol{\theta}^T\boldsymbol{h} - \delta\boldsymbol{E}^T\boldsymbol{D})dV = \delta L_{ext} \tag{20}$$

If geometrical and constitutive equation are substituted in Equation 20 the following equation is obtained:

$$\begin{aligned}\delta L_{int} = \int_V (&\delta\boldsymbol{\varepsilon}^T\boldsymbol{C}\boldsymbol{\varepsilon} - \delta\boldsymbol{\varepsilon}^T\boldsymbol{\lambda}\vartheta - \delta\boldsymbol{\varepsilon}^T\boldsymbol{e}\boldsymbol{E} + \delta\boldsymbol{\theta}^T\boldsymbol{\kappa}\boldsymbol{\theta} + \\ &-\delta\boldsymbol{E}^T\boldsymbol{e}\boldsymbol{\varepsilon} - \delta\boldsymbol{E}^T\boldsymbol{\chi}\boldsymbol{E} - \delta\boldsymbol{E}^T\boldsymbol{p}\vartheta)dV\end{aligned} \tag{21}$$

If the kinematic approximation introduced before is used the terms that compose the virtual variation of the internal work can be written in matrix form.

The first term, $\delta\boldsymbol{\varepsilon}^T\boldsymbol{C}\boldsymbol{\varepsilon}$, represents the mechanical problem. The strain can be expressed in therm of derivatives of the displacements, moreover the displacements can be written using the shape functions N_i and F_τ.

$$\begin{aligned}\delta\boldsymbol{\varepsilon}^T\boldsymbol{C}\boldsymbol{\varepsilon} =& \delta\boldsymbol{q}_{\boldsymbol{u}_{js}}^T \int_V N_j F_s \boldsymbol{I}\boldsymbol{D}_u^T\boldsymbol{C}\boldsymbol{D}_u\boldsymbol{I}F_\tau N_i dV \boldsymbol{q}_{\boldsymbol{u}_{i\tau}} = \\ =& \delta\boldsymbol{q}_{\boldsymbol{u}_{js}}^T \boldsymbol{k}_{uu}^{ij\tau s}\boldsymbol{q}_{\boldsymbol{u}_{i\tau}}\end{aligned} \tag{22}$$

$\boldsymbol{k}_{uu}^{ij\tau s}$ is the fundamental nucleus of size 3×3 of the stiffness matrix of the pure mechanical problem. $\boldsymbol{q}_{\boldsymbol{u}_{i\tau}}$ is the part of the unknown vector related to the mechanical variables.

The term $\delta\boldsymbol{\varepsilon}^T\boldsymbol{\lambda}\vartheta$ can be written as:

$$\begin{aligned}\delta\boldsymbol{\varepsilon}^T\boldsymbol{\lambda}\vartheta =& \delta\boldsymbol{q}_{\boldsymbol{u}_{js}}^T \int_V N_j F_s \boldsymbol{I}\boldsymbol{D}_u^T\boldsymbol{\lambda}\boldsymbol{I}F_\tau N_i dV \boldsymbol{q}_{\boldsymbol{\vartheta}_{i\tau}} = \\ =& \delta\boldsymbol{q}_{\boldsymbol{u}_{js}}^T \boldsymbol{k}_{u\theta}^{ij\tau s}\boldsymbol{q}_{\boldsymbol{u}_{i\tau}}\end{aligned} \tag{23}$$

$\boldsymbol{k}_{u\theta}^{ij\tau s}$ is the fundamental nucleus of size 3×1 of the stiffness matrix of the thermo-elastic problem. $\boldsymbol{q}_{\boldsymbol{\vartheta}_{i\tau}}$ is the part of the unknown vector related to the thermal variable.

The term $\delta\boldsymbol{\varepsilon}^T\boldsymbol{e}\boldsymbol{E}$ can be written as:

$$\begin{aligned}\delta\boldsymbol{\varepsilon}^T\boldsymbol{e}\boldsymbol{E} =& \delta\boldsymbol{q}_{\boldsymbol{u}_{js}}^T \int_V N_j F_s \boldsymbol{I}\boldsymbol{D}_u^T\boldsymbol{e}\boldsymbol{D}_\phi\boldsymbol{I}F_\tau N_i dV \boldsymbol{q}_{\boldsymbol{\phi}_{i\tau}} = \\ =& \delta\boldsymbol{q}_{\boldsymbol{u}_{js}}^T \boldsymbol{k}_{u\phi}^{ij\tau s}\boldsymbol{q}_{\boldsymbol{u}_{i\tau}}\end{aligned} \tag{24}$$

$\boldsymbol{k}_{u\phi}^{ij\tau s}$ is the fundamental nucleus of size 3×1 of the stiffness matrix of the piezo-elastic problem. $\boldsymbol{q}_{\boldsymbol{\phi}_{i\tau}}$ is the part of the unknown vector related to the electrical variable.

The term $\delta\boldsymbol{\theta}^T\boldsymbol{\kappa}\boldsymbol{\theta}$ can be written as:

$$\begin{aligned}\delta\boldsymbol{\theta}^T\boldsymbol{\kappa}\boldsymbol{\theta} =& \delta\boldsymbol{q}_{\boldsymbol{\vartheta}_{js}}^T \int_V N_j F_s \boldsymbol{I}\boldsymbol{D}_\vartheta^T\boldsymbol{\kappa}\boldsymbol{D}_\vartheta\boldsymbol{I}F_\tau N_i dV \boldsymbol{q}_{\boldsymbol{\vartheta}_{i\tau}} = \\ =& \delta\boldsymbol{q}_{\boldsymbol{u}_{js}}^T \boldsymbol{k}_{\theta\theta}^{ij\tau s}\boldsymbol{q}_{\boldsymbol{u}_{i\tau}}\end{aligned} \tag{25}$$

$\boldsymbol{k}_{\theta\theta}^{ij\tau s}$ is the fundamental nucleus of size 1×1 of the stiffness matrix of the pure thermal problem.

The term $\delta \boldsymbol{E}^T \boldsymbol{e\varepsilon}$ can be written as:

$$\begin{aligned}\delta \boldsymbol{E}^T \boldsymbol{e\varepsilon} =& \delta \boldsymbol{q}_{\boldsymbol{\phi}_{js}}^T \int_V N_j F_s \boldsymbol{I} \boldsymbol{D}_\phi^T \boldsymbol{e} \boldsymbol{D}_u \boldsymbol{I} F_\tau N_i dV \boldsymbol{q}_{\boldsymbol{u}_{i\tau}} = \\ =& \delta \boldsymbol{q}_{\boldsymbol{\phi}_{js}}^T \boldsymbol{k}_{\phi u}^{ij\tau s} \boldsymbol{q}_{\boldsymbol{u}_{i\tau}}\end{aligned} \tag{26}$$

$\boldsymbol{k}_{\phi u}^{ij\tau s}$ is the fundamental nucleus of size 1×3 of the stiffness matrix of the piezo-elastic problem.

The term $\delta \boldsymbol{E}^T \boldsymbol{\chi} \boldsymbol{E}$ can be written as:

$$\begin{aligned}\delta \boldsymbol{E}^T \boldsymbol{\chi} \boldsymbol{E} =& \delta \boldsymbol{q}_{\boldsymbol{\phi}_{js}}^T \int_V N_j F_s \boldsymbol{I} \boldsymbol{D}_\phi^T \boldsymbol{\chi} \boldsymbol{D}_\phi \boldsymbol{I} F_\tau N_i dV \boldsymbol{q}_{\boldsymbol{\phi}_{i\tau}} = \\ =& \delta \boldsymbol{q}_{\boldsymbol{\phi}_{js}}^T \boldsymbol{k}_{\phi\phi}^{ij\tau s} \boldsymbol{\phi}_{i\tau}\end{aligned} \tag{27}$$

$\boldsymbol{k}_{\phi\phi}^{ij\tau s}$ is the fundamental nucleus of size 1×1 of the stiffness matrix of the pure electric problem.

The term $\delta \boldsymbol{E}^T \boldsymbol{p} \vartheta$ can be written as:

$$\begin{aligned}\delta \boldsymbol{E}^T \boldsymbol{p} \vartheta =& \delta \boldsymbol{q}_{\boldsymbol{\phi}_{js}}^T \int_V N_j F_s \boldsymbol{I} \boldsymbol{D}_\phi^T \boldsymbol{p} \boldsymbol{D}_\theta \boldsymbol{I} F_\tau N_i dV \boldsymbol{q}_{\boldsymbol{\theta}_{i\tau}} = \\ =& \delta \boldsymbol{q}_{\boldsymbol{\phi}_{js}}^T \boldsymbol{k}_{\phi\theta}^{ij\tau s} \boldsymbol{\theta}_{i\tau}\end{aligned} \tag{28}$$

$\boldsymbol{k}_{\phi\theta}^{ij\tau s}$ is the fundamental nucleus of size 1×1 of the stiffness matrix of the pyro-electric problem.

All the fundamental nucleus can be assembled together in fundamental nucleus of the multi-field problem:

$$\delta L_{int} = \delta \boldsymbol{q}_{js}^T \overbrace{\begin{bmatrix} \begin{bmatrix} \ddots & & \\ & \boldsymbol{k}_{uu} & \\ & & \ddots \end{bmatrix} & \begin{bmatrix} \vdots \\ \boldsymbol{k}_{u\theta} \\ \vdots \end{bmatrix} & \begin{bmatrix} \vdots \\ \boldsymbol{k}_{u\phi} \\ \vdots \end{bmatrix} \\ \begin{bmatrix} \cdots & 0 & \cdots \end{bmatrix} & \begin{bmatrix} \boldsymbol{k}_{\theta\theta} \end{bmatrix} & \begin{bmatrix} 0 \end{bmatrix} \\ \begin{bmatrix} \cdots & \boldsymbol{k}_{\phi u} & \cdots \end{bmatrix} & \begin{bmatrix} K_{\phi\theta} \end{bmatrix} & \begin{bmatrix} \boldsymbol{k}_{\phi\phi} \end{bmatrix} \end{bmatrix}}^{\boldsymbol{k}^{ij\tau s}} \boldsymbol{q}_{i\tau} \tag{29}$$

The contributions $\boldsymbol{k}_{\theta\phi}$ and $\boldsymbol{k}_{\theta u}$ can be neglected when an external temperature is imposed as boundary condition, as in the present paper.

Loading Vector

The virtual work, due to a mechanical point load $\boldsymbol{P}$, can be written as:

$$\delta L_{ext} = \boldsymbol{P} \delta \boldsymbol{u}^T \tag{30}$$

By introducing the nodal displacements and the shape functions, the previous equation becomes

$$\delta L_{ext} = F_\tau N_i \boldsymbol{P} \delta \boldsymbol{q}_{u_{js}}^T \tag{31}$$

Rotation and assembly of the fundamental nucleus

The analysis of complex structures requires finite elements to be rotated in any direction and the stiffness to be computed in a given reference system, that is, the displacements have to be expressed in the same, global reference system. The matrices can be written in the global reference system using a rotation matrix, with respect to the local reference system. The rotation matrices are:

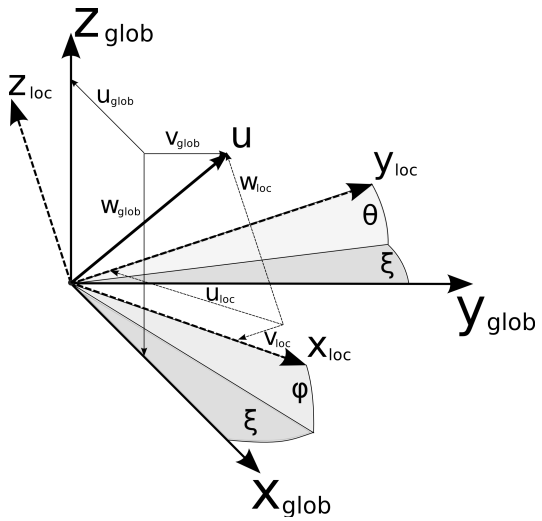

Figure 2. Representation of the rotation angles.

$$\boldsymbol{\Lambda_x} = \begin{bmatrix} 1 & 0 & 0 \\ 0 & cos(\theta) & sin(\theta) \\ 0 & -sin(\theta) & cos(\theta) \end{bmatrix}, \tag{32}$$

$$\boldsymbol{\Lambda_y} = \begin{bmatrix} cos(\phi) & 0 & sin(\phi) \\ 0 & 1 & 0 \\ -sin(\phi) & 0 & cos(\phi) \end{bmatrix}, \tag{33}$$

$$\boldsymbol{\Lambda_z} = \begin{bmatrix} cos(\xi) & -sin(\xi) & 0 \\ sin(\xi) & cos(\xi) & 0 \\ 0 & 0 & 1 \end{bmatrix} \tag{34}$$

where θ, ϕ and ξ are the rotation angles around the x,y,and z axis, as shown in Fig. 2 The displacement vector in the global reference system, $\boldsymbol{u}_{glob}$, can be written as:

$$\boldsymbol{u}_{glob} = \boldsymbol{\Lambda_x} \boldsymbol{\Lambda_y} \boldsymbol{\Lambda_z} \boldsymbol{u}_{loc} = \boldsymbol{\Lambda} \boldsymbol{u}_{loc} \tag{35}$$

Therefore, the mechanical part of the fundamental nucleus in the global reference system becomes:

$$\boldsymbol{k}_{uu_{glob}}^{ij\tau s} = \boldsymbol{\Lambda}^T \boldsymbol{k}_{uu_{loc}}^{ij\tau s} \boldsymbol{\Lambda} \tag{36}$$

The coupling terms can be rotated using the following equations:

$$\boldsymbol{k}_{u\Theta_{glob}}^{ij\tau s} = \boldsymbol{\Lambda}^T \boldsymbol{k}_{u\Theta_{loc}}^{ij\tau s} \tag{37}$$

$$\boldsymbol{k}_{u\phi_{glob}}^{ij\tau s} = \boldsymbol{\Lambda}^T \boldsymbol{k}_{u\phi_{loc}}^{ij\tau s} \tag{38}$$

$$\boldsymbol{k}_{\phi u_{glob}}^{ij\tau s} = \boldsymbol{k}_{\phi u_{loc}}^{ij\tau s^T} \boldsymbol{\Lambda} \tag{39}$$

The terms $\boldsymbol{k}_{\phi\phi}$, $\boldsymbol{k}_{\phi\theta}$ and $\boldsymbol{k}_{\theta\theta}$ are related to scalar fields therefore do not need to be rotated. Once all the elements have been expressed in the same reference system, the global stiffness matrix can be assembled using the classical FEM approach.

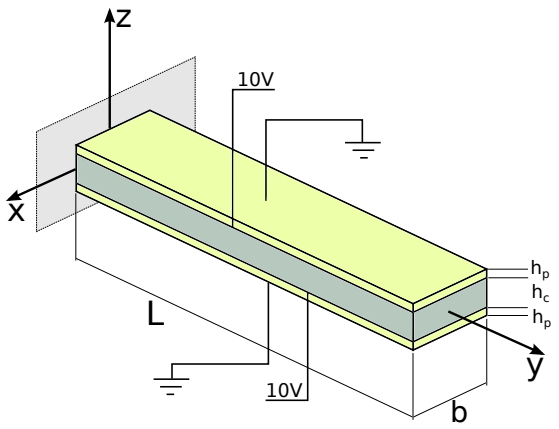

Figure 3. Geometry of the sandwich beam used in the piezo-elastic assessment

PZT-5H		
Mechanical properties		
C_{22}	126	GPa
C_{12}	79.5	GPa
C_{13}	84.1	GPa
C_{33}	117	GPa
C_{44}	23	GPa
Piezoelectric properties		
e_{32}	-6.5	Cm^{-2}
e_{33}	23	Cm^{-2}
e_{25}	17	Cm^{-2}
χ_{22}	1.5045	$C^2N^{-1}m^2$
χ_{33}	1.3009	$C^2N^{-1}m^2$

Table 1. PZT-5H Piezoceramic material properties

aluminum alloy 1		
Mechanical properties		
E	70.3	GPa
ν	0.345	-

Table 2. aluminum alloy 1 material properties

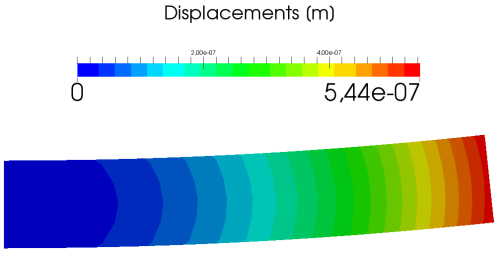

Figure 4. Displacement field of the sandwich beam at x=0.

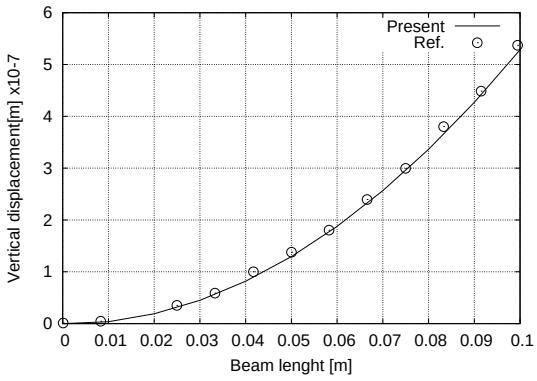

Figure 5. Vertical displacement of the beam along the y-axis.

Numerical Results

The results obtained using the previously introduced structural model are reported in this section. In the first part, the structural model has been assessed, and the results have been compared with those present in literature. Piezo-elastic and thermo-piezo-elastic models have been considered. In the second part the performances of two amplified piezoelectric actuators have been investigated.

Piezo-elastic model assessment

The piezo-elastic model has been assessed in this section. The sandwich beam considered in the analysis is shown in Figure 3. The beam has a length, L, of 0.1 m, the thickness of the metallic core, h_c, is 16 mm and the two external piezo-patches have a thickness, h_p, equal to 1 mm. The width is considered equal to 1 m. A potential of 10V is applied at the interface face between the piezoelectric patch and the internal core, while, the external free faces have a potential set equal to 0V. The piezoelectric patches are polarized in the z direction.

The properties of the piezoelectric material used in the patches are reported in Table 1, while the properties of the aluminum alloy used in the core are reported in Table 2.

The displacements due to the applied voltage, have been evaluated. The results have been compared with those of Zhang and Sun (1996).

Figure 4 show the displacement considering a slice at x=0. The piezoelectric patch produces the bending of the beam.

Figure 5 shows the vertical displacement of the beam along the length of the beam. The results are in agreement with those present in literature. This assessment proves that the present beam formulation is able to provide an accurate description of piezo-elastic coupling.

Thermo-piezo-elastic model assessment

In this section the fully coupled thermo-piezo-elastic model has been assessed. The structure reported in Figure 7 has been considered. This is once again a sandwich beam but with the following dimensions: L equal to 1 m, b equal to 0.0508 m, the core thickness, h_c, equal to 3.36 mm and the thickness of two external piezo-patches, h_p,is equal to 0.254 mm.

The internal core has the properties that are reported in Table 3, while the external piezoelectric patches have been built using the same material that was used in the previous assessment, that is PZT-5H. The thermal properties of this material are reported in Table 4.

The structure is subject to a constant temperature, and the interfaces between the core and the patches are forced to have an electric potential of 0V. The voltage of the external layer faces, due to the deformation caused by the thermal load, has been evaluated. The results have been compared with those of Tzou and Ye (1994).

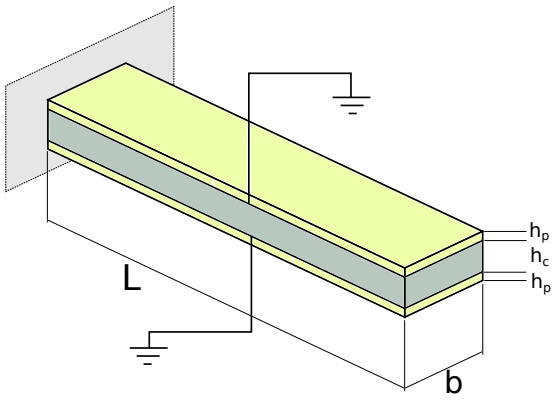

Figure 6. Geometry of the sandwich beam used in the thermo-piezo-elastic assessment

aluminum alloy 1		
Mechanical properties		
E	68.95	GPa
ν	0.292	-
Thermal properties		
α	11×10^{-6}	$^oC^{-1}$

Table 3. aluminum alloy 2 material properties

PZT-5H		
Thermal properties		
λ_1	2×10^5	$Nm^2\ ^oC^{-1}$
λ_2	2×10^5	$Nm^2\ ^oC^{-1}$
λ_3	-2.7×10^5	$Nm^2\ ^oC^{-1}$
Pyro-electric properties		
p_3	25×10^{-6}	$Cm^2\ ^oC^{-1}$

Table 4. PZT-5H material thermal properties

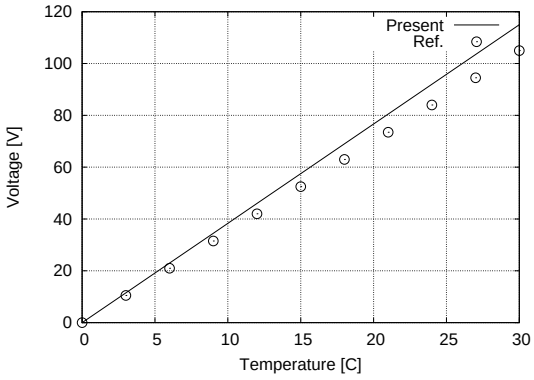

Figure 7. Upper face potential at different temperature.

Figure 7 shows the variation of the electric potential at different temperatures. It is possible to see that there is a linear correlation between the temperature and the potential. The small difference between the present results and the reference values is due to the different kinematic model that has been adopted. While the reference results were obtained using classical models, the present approach takes into account a *quasi* three-dimensional deformation that produces a slightly higher potential.

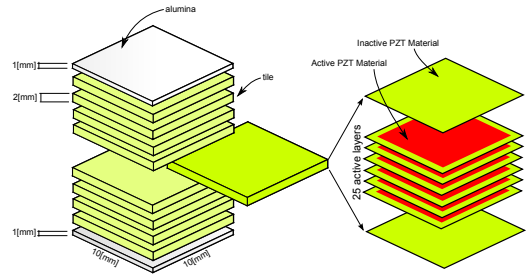

Figure 8. MLA geometry and layers set-up.

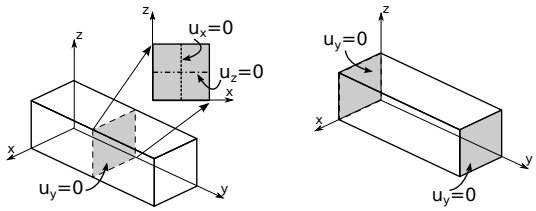

(a) *Free-stroke evaluation* (b) *Blocking force evaluation*

Figure 9. Models boundary conditions

Multi-layered piezoelectric stack analysis

The use of a Multi-Layered Actuator (MLA) allows a strong electric field to be applied without the need of excessively high voltages. These actuators are made up of a stack of tiles, as shown in figure 8, each of which has to be connected to an electric supply. In this section, a Multi-layered stack has been investigated. Two different materials are considered: a soft doped piezoceramic material (HT-S) and a hard doped material (HT-H). The mechanical material properties and the behavior at high temperature have been investigate during the AeroPZT project activities and have been presented by Mangeot (2015). The properties of these materials are reported in Table 5. The MLA has a square cross-section, as shown in Figure 8, with a 0.01 m edge. The length of the stack is 0.02 m. The free stroke and the blocking force have been investigated. A voltage of 200V has been applied, that is, in according with the geometrical properties of the actuator, the active material is subject to an electric field equal to 2985 kV/m that is in the operational limits of the material as shown in the work by Mangeot and Andersen (2016). When the free stroke was considered, the model was constrained in the central section, but the section deformation was not constrained, as shown in Figure 9a. The blocking force has been evaluated imposing zero displacements at the two ends, see Figure 9b. The results have been compared with those obtained from the experimental test performed by NOLIAC. An accurate FEM model has been considered, and each tile has been modeled separately in order to describe the internal behavior of the material in detail. The cross section has been discretized using 9 L9 elements. The results are reported in Table 6. The present model is able to accurately predict the behavior of the material. The obtained results are included in the tolerance range reported in the datasheet and are in agreement with the experimental results. Because of its better dynamic performances the HT-H material will be used in the subsequent models. The one-dimensional model

	E11	E33	ν	ρ	$e15$	$e24$	$e31$	$e32$	$e33$	$\epsilon 11$	$\epsilon 22$	$\epsilon 33$
	GPa	Gpa	-	$[Kg/m^3]$	C/m^2	C/m^2	C/m^2	C/m^2	C/m^2	F/m	F/m	F/m
HT-S	46	30	0.39	7708	13.7	13.7	-6.06	-6.06	17.2	1.72E-8	1.72E-8	1.68E-8
HT-H	54	35	0.334	7700	8	8	-4	-4	10.8	1.72E-8	1.72E-8	1.68E-8

Table 5. Piezoceramic material properties

	HT-S			HT-H		
	Present	Test	Data-Sheet	Present	Test	Data-Sheet
Free stroke	30.2 μm	32 μm	[27.6 μm +/ − 20%]	16.6 μm	18.4 μm	[18.0 μm +/ − 20%]
Blocking Force	4006 N	-	[4200N +/ − 20%]	2600 N	-	[3200 N +/ − 20%]

Table 6. Performances of the MLA actuators

used in the present analysis appears to be reliable and has therefore been used in the subsequent analyses.

Amplified Piezoceramic Actuator (APA) analysis

Piezoceramic actuators produce a high blocking force but a small free stroke, as shown in the previous section. When these actuators have to be used in applications that require higher displacements an amplification device is required. The amplified piezoceramic actuator (APA) is able to amplify the free strok, thus reducing the blocking force. Figure 10 shows the geometry of an APA device. The maximum dimension of the device is $0.15m$, while each stack is $0.02m$ long. A stack of piezoceramic elements is contained within an external shell which provides the amplification. The amplification factor can be modified using a different shell geometry. A metallic wedge is included between the piezoceramic elements in order to provide the correct pre-stress value necessary for dynamic application. The external shell and the wedge of the APA

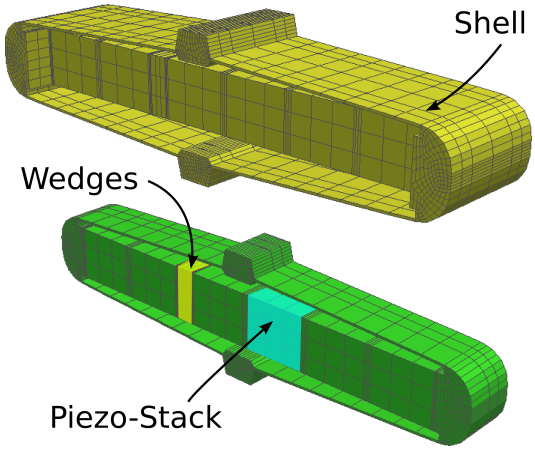

Figure 10. Amplified Piezoelectric Actuator Model

considered in this section are built in aluminum, while, the piezoceramic stacks are built using the previously presented HT-H material. Figure 11 shows the approach that was adopted to build the numerical model using the present one-dimensional model. Beam elements have been used along the axis of the piezoceramic stacks, while the external shell has been modeled using the beam elements in the transversal direction. In the case of the piezoceramic stacks the polarization axis coincides with the beam axis. The blocking force and the free stroke have been evaluated. The results are reported in Table 7, while Figure 12 shows the

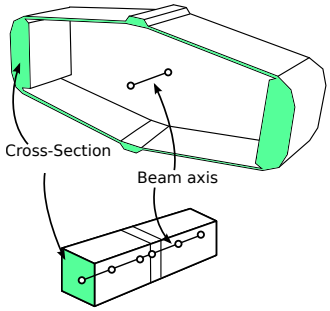

Figure 11. Amplified Piezoelectric Actuator beam model

Blocking Force $[N]$	Free Stroke [m]
~ 118	-0.00185

Table 7. APA performances

displacement field of the APA actuator when it is activated at the maximum voltage of 200 V, that is in the free stroke condition. Figure 12 shows the strain ϵ_{xx} distribution in the free stroke condition.

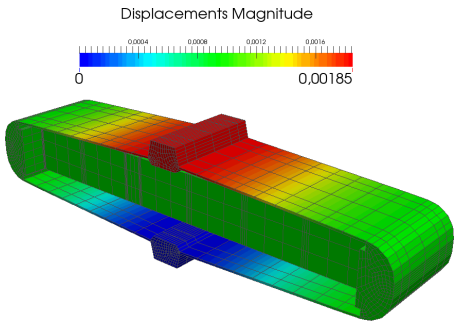

Figure 12. Displacement field of the APA actuator during the free stroke analysis

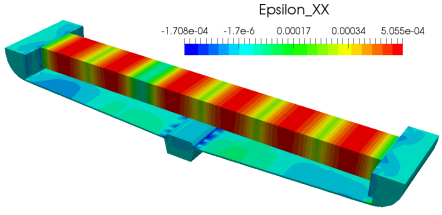

Figure 13. ϵxx strain of the APA actuator during the free stroke analysis

Temperature	Displ
	mm
-80^oC	+1.22
-40^oC	+0.73
0^oC	+0.16
100^oC	+0.11
180^oC	+0.82
250^oC	+1.82

Table 8. vertical displacement of the APA actuator at different temperature

The use of an APA actuator at high temperatures may lead to a large thermal deformation because the values of the thermal expansion coefficients, CTE, of the used materials are very different. While the aluminum has an almost constant CTE, the piezoceramic material has a CTE value that varies according to the temperature. Moreover, it is usually much lower than the CTE of the aluminum. In the present work the CTE of aluminum has been considered constant with a value of $23 \times 10^{-6}\ {}^oC^{-1}$, while, the values of the CTE for the piezoceramic materials have been investigated by CEDRAT during the project activities. Table 8 reports the displacement of the APA actuator when is subject to a constant temperature. The results show that the device may have a higher deformation than he free stroke at higher temperatures, that is, the thermal load makes the actuation vanish completely.

Figure 14 shows the displacement field of the APA actuator when it is subjected to a temperature of 180^oC.

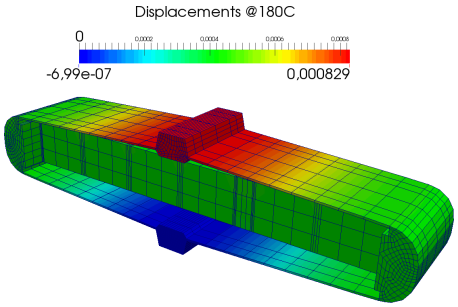

Figure 14. APA displacement field at 180^oC

Super Amplified Piezoceramic Actuator (sAPA) analysis

When a smaller device has to reach a higher amplification factor, a Super Amplified Piezoelectric Actuator, S-APA, can be used. Figure 15 shows the S-APA configuration, in this case the maximum dimension of the device is lower than 0.1 m . The same principle as that of the APA is used/adopted, but more amplification shells are used in order to increase the amplification factor. Because of the problems due to the thermal loads, that emerged during the APA analysis, the shells of the present model have been built in Invar, in order to reduce the effects of the thermal load. The wedges between the piezoceramic stack have been built in aluminum. HT-H piezo-ceramic material has been used in the piezo-stack. The same modeling approach as that used for the APA model has been used, and the piezoceramic elements have

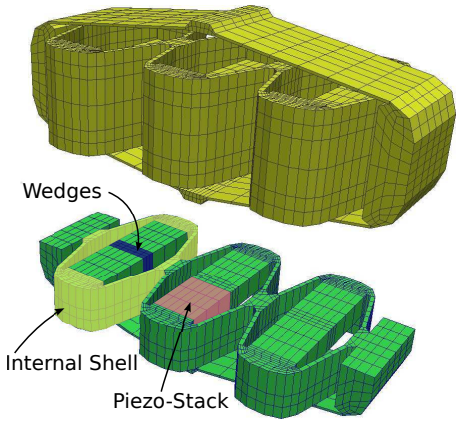

Figure 15. Super Amplified Piezoelectric Actuator Model

been modeled using the beam elements on the stack axis while the shells have been modeled using the beam elements in the transversal direction, as shown in Figure 11. The

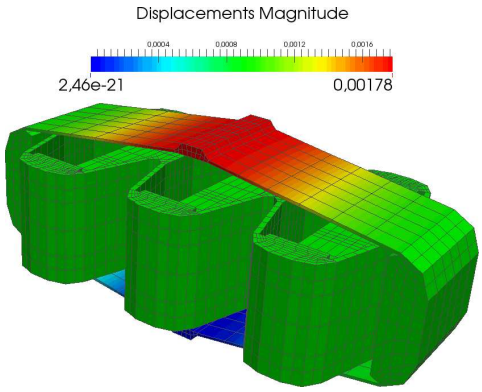

(a) Free Stroke Analysis

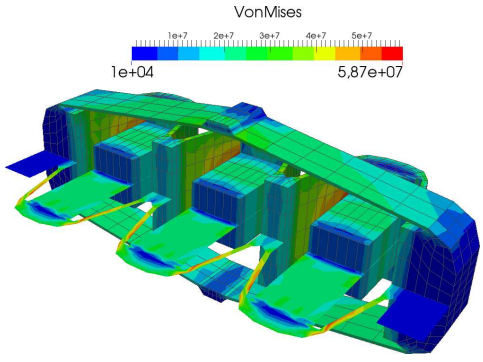

(b) Von Mises Stress at the blocking force

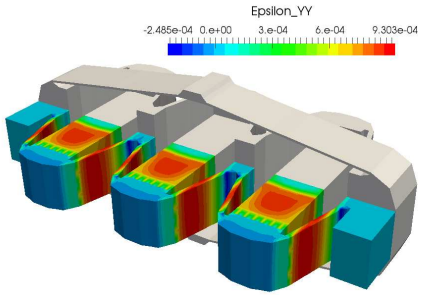

(c) ϵ_{yy} strain at the free stroke

Figure 16. Super Amplified Piezoelectric Actuator Model Performances

Blocking Force $[N]$	Free Stroke [m]
$\sim$118 (114)	0.00178 (0.00183)

Table 9. Super-APA performances

Temperature	Displ
	mm
-80^oC	-1.04
-40^oC	-0.63
0^oC	-0.10
100^oC	-0.03
180^oC	-1.11
250^oC	-2.22

Table 10. Super-APA max displacement at different temperatures

free stroke and the blocking force of the actuator have been investigated. Both values have been evaluated considering that the maximum voltage, 200V, was applied at the piezoceramic stack, that is, the active material is subject to an electric field equal to 2985 kV/m

Table 9 reports the numerical results, the reference values obtained by Cedrat Technologies, a partner of the AeroPZT project, using a commercial code,are reported in brackets. Figures 16a and 16b report the displacement field when the free stroke was evaluated, and the Von Mises stress during the blocking force analysis. Figure 16c reports the $\epsilon_{(yy)}$ in the free stroke condition.

The thermal response of the structure has also been investigated. The displacements due to a constant temperature distribution have been evaluated considering changes in the thermal properties of the material due to variations of the temperature. Table 10 reports the displacements in the upper part of the S-APA device due to the thermal load. Figures 17 reports the displacement field at 180^oC, that is the upper limit of the operability range of the device.

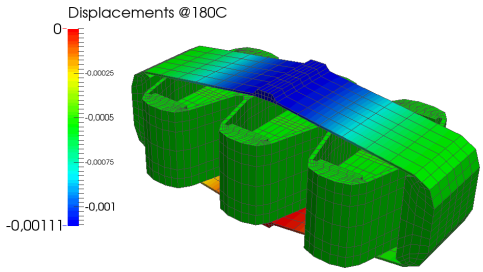

Figure 17. Super Amplified Piezoelectric Actuator Thermal analysis at $+180^oC$

The results of the thermal analysis show that the model is affected to a great extent by the thermal effects. The large difference between the CTE of the used materials and the high amplification factor, due to the adopted device configuration, make the thermal aspects critical. The displacements due to the thermal loads t the limit of the operability range ($-40^oC \div 180^oC$) are lower than the free stroke, that is, the device is operative over the whole range of temperature even when the performances are reduced.

The use of a combination of alternative materials has also been investigated in order to reduce the thermal deformation

shell	Invar	Steel	All.	Steel
wedges	All.	All.	All.	Invar
-40^oC	-0.63	-1.05	-1.82	-0.825
180^oC	-1.11	-0.22	+1.26	-0.83

Table 11. Displacement (mm) at the limit operability temperatures for different Super-APA configuration

of the device. Neither the piezoceramic stacks nor the internal shells have not been modified. The two parts of the actuator that have been modified are the external shell and the wedges between the piezoceramic stacks. Steel and aluminum have been considered as possible alternatives to Invar in the external shell while the wedges have also been considered in aluminum. The results reported in Table 11 show that the use of different materials could lead to notable variations in the performances of the device. In particular, the use of Steel for the external shell and Invar for the wedge could led to an almost symmetrical response at high and low temperatures. The use of a higher CTE material in the external shell may lead to a compensation of the displacements due to the thermal loads.

Conclusions

An advanced thermo-piezo-elastic one-dimensional model is presented in the present work. The computational model has been developed in the frameworks of the Carrera Unified Formulation, which allows refined structural models to be derived in a compact form. A fully-coupled multi-field model is presented. Numerical assessments have been used to demonstrate its accuracy. The model has been used to perform thermo-piezo-elastic analyses of two amplified piezoceramic actuators. The design of these devices has been developed within the AeroPZT project, in the frameworks of the CleanSKY program. The analyses have focused on the prediction of the piezo-elastic response of the devices and on the effect of the thermal load on the performances of the actuator. The following major conclusions can be drawn:

- The present numerical model is able to accurately predict the thermo-piezo-elastic response.
- The refined one-dimensional models can be used in the analysis of complex structures such as that of amplified piezoelectric actuators.
- Thermal effects represent a critical point in the actuator design and cannot be neglected.
- The use of low CTE materials allows the thermal effects to be reduced, which in turn allows the range of operability of the devices to be extended.

In conclusion the present model has been proved to be reliable for the analysis of complex piezoelectric device. The thermal effects appear to be a critical point in the design of amplified piezoceramic actuators because of the large differences in the thermal expansion coefficients of the material. An accurate numerical analysis allows the thermo-piezo-elastic response to be predicted and the design to be improved in order to extend the use of such devices i high temperature applications.

Acknowledgement

Part of this work has been done in the framework of the European project FP7: AeroPZT, grant agreement: 632604. Erasmo Carrera has partially been supported by RSF Grant No. 15-19-30002.

References

Ahmad SN, Upadhyay CS and Venkatesan C (2006) Electro-thermo-elastic formulation for the analysis of smart structures. *Smart Materials and Structures* 15(2): 401.

Bailey T and Hubbard J (1985) Distributed piezoelectric polymer active vibration control of a cantilever beam. *AIAA Journal* (8): 605–611.

Biscani F, Nali P, Belouettar S and Carrera E (2012) Coupling of hierarchical piezoelectric plate finite elements via arlequin method. *Journal of intelligent materials systems and structures* (23): 749.

Carrera E (1997) An improved reissner-mindlin-type model for the electromechanical analysis of multilayered plates including piezo-layers. *JOURNAL OF INTELLIGENT MATERIAL SYSTEMS AND STRUCTURES* 8: 232–248.

Carrera E (2000) An assessment of mixed and classical theories for thermal stress analysis of orthotropic multilayered plates. *JOURNAL OF THERMAL STRESSES* 23: 797–831.

Carrera E (2003) Theories and finite elements for multilayered plates and shells: A unified compact formulation with numerical assessment and benchmarking. *ARCHIVES OF COMPUTATIONAL METHODS IN ENGINEERING* 10: 215–297.

Carrera E and Boscolo M (2007) Hierarchic multilayered plate elements for coupled multifield problems of piezoelectric adaptive structures: Formulation and numerical assessment. *ARCHIVES OF COMPUTATIONAL METHODS IN ENGINEERING* 14(4): 383–430.

Carrera E, Boscolo M and Robaldo A (2007) Hierarchic multilayered plate elements for coupled multifield problems of piezoelectric adaptive structures: Formulation and numerical assessment. *ARCHIVES OF COMPUTATIONAL METHODS IN ENGINEERING* 14(4): 383–430.

Carrera E, Brischetto S and Nali P (2008) Variational Statements and Computational Models for MultiField Problems and Multilayered Structures. *Mechanics of Advanced Materials and Structures* 15(3-4): 182–198. DOI:10.1080/15376490801907657.

Carrera E, Cinefra M, Petrolo M and Zappino E (2014) Comparisons between 1d (beam) and 2d (plate/shell) finite elements to analyze thin walled structures. *Aerotecnica Misssili & Spazio. The journal of Aerospace Science, Technology and Systems* 93(1-2).

Carrera E, Gaetano G and M P (2011a) *Beam Structures, Classical and Advanced Theories.* John Wiley & Sons.

Carrera E, Giunta G, Nali P and Petrolo M (2010) Refined beam elements with arbitrary crpss-section geometries. *Computers and Structures* (88): 283–293.

Carrera E and Petrolo M (2012) Refined beam elements with only displacement variables and plate/shell capabilities. *Meccanica* 47: 537–556.

Carrera E, Petrolo M and Nali P (2011b) Unified formulation applied to free vibrations finite element analysis of beams with arbitrary section. *Shock and vibrations* 18(3): 485–502.

Carrera E, Petrolo M and Varello A (2012a) Advanced beam formulations for free vibrations analysis of conventional and joined wings. *Journal of aerospace engineering* 25(2): 282–293.

Carrera E and Robaldo A (2007) Extension of reissner mixed variational principle to thermopiezelasticity. *ATTI DELLA ACCADEMIA DELLE SCIENZE DI TORINO. CLASSE DI SCIENZE FISICHE MATEMATICHE E NATURALI* 31: 27–42.

Carrera E, Zappino E and Petrolo M (2012b) Advanced elements for the static analysis of beams with compact and bridge-like sections. *Journal of structural engineering* (56): 49–61.

Caruso G, Galeani S and Menini L (2003) Active vibration control of an elastic plate using multiple piezoelectric sensors and actuators. *Simulation modelling prectice and theory* (11): 403–419.

Crawley E and Luis J (1987) Use of piezoelectric actuators as elements of intelligent structures. *AIAA Journal* (25): 1373–1385.

Dong XJ, Meng G and Peng JC (2006) Vibration control of piezoelectric actuators smart structures based on system identification technique. *Journal of sound and vibration* (297): 680–693.

Kim TW and Kim JH (2005) Optimal distribution of an active layer for transient vibration control of an flexible plates. *Smart material and Structures* (14): 904–916.

Kumar K and Narayanan S (2007) The optimal location of piezolectric actuators and sensors for vibration controls of plate. *Smart material and structures* (16): 2680–2691.

Kusculuoglu ZK and Royston TJ (2005) Finite element formulation for composite plates with piezoceramic layers for optimal vibration control applications. *Smart material and structures* (14): 1139–1153.

Liu G, Dai K and Lim K (2004) Static and vibration control of composite laminates integrated with piezoelectric sensors and actuators using radial point interpolation method. *Smart material and structures* (14): 1438–1447.

Mangeot C (2015) Temperature dependence of soft/hard pzt material properties and impact on the design. In: *12th International Workshop on Piezoelectric Materials and Applications in Actuators*, volume 12th International Workshop on Piezoelectric Materials and Applications in Actuators. Vilnius, Lithuania, 29 June1 July.

Mangeot C and Andersen B (2016) Investigation of large signal properties of quasi-static lead zirconate titanate actuators at elevated temperature. *Advances in Applied Ceramics* 115(2): 72–76. DOI:10.1080/17436753.2015.1104051.

Miglioretti F, Carrera E and Petrolo M (2014) Variable kinematic beam elements for electro-mechanical analysis. *Smart Structures and Systems* 13(4): 517–546.

Moita J, Soares C and Soares C (2005) Active control of forced vibration in adaptive structures using a higher order model. *Composite structures* (71): 349–355.

Moitha J, Correira I, Soares C and Soares C (2004) Active control of adaptive laminated structures with bonded piezoelectric sensors and actuators. *Computer and Structures* (82): 1349–1358.

Robaldo A, Carrera E and Benjeddou A (2005) Unified formulation for finite element thermoleastic analysis of multilayered anisotropic composite plates. *JOURNAL OF THERMAL*

STRESSES 28: 1031–1064.

Robaldo A, Carrera E and Benjeddou A (2006) A unified formulation for finite element analysis of piezoelectric plates. *COMPUTERS & STRUCTURES* 84: 1494–1505.

Sarvanos D and Heyliger P (1999) Mechanics and computational models for laminated piezoelectric beams, plate, and shells. *Applied mechanic review* 52(10): 305–320.

Tzou HS and Ye R (1994) Piezothermoelasticity and precision control of piezoelectric systems: Theory and finite element analysis. *Journal of Vibration and Acoustics* 116(4): 489–495.

Vasques C and Rodrigues J (2006) Active vibration of smart piezoelectric beams: comparison of classical and optimal feedback control strategies. *Computer and Structures* (84): 1459–1470.

Vidal P, D'Ottavio M, Thaier M and Polit O (2011) An efficient finite shell element for the static resposne of piezoelectric laminates. *Journal of intelligent materials systems and structures* (22): 671.

Xu S and Koko T (2004) Finite element analysis and design of actively acontrolled piezoelectric smart structure. *Finite element in Analysis and Design* (40): 241–262.

Zappino E, Carrera E, Rowe S, Mangeot C and Marques H (2016) Numerical analyses of piezoceramic actuators for high temperature applications. *Composite Structures* 151: 36 – 46. DOI:http://dx.doi.org/10.1016/j.compstruct.2016.01.084. Smart composites and composite structures In honour of the 70th anniversary of Professor Carlos Alberto Mota Soares.

Zhang XD and Sun CT (1996) Formulation of an adaptive sandwich beam. *Smart Materials and Structures* 5(6): 814.

Zhou X, Chattopadhyay A and Gu H (2000) Dynamic resposne of smart composites using a coupled thermo-piezoelectric-mechanical model. *AIAA Journal* (38): 1939–1948.

Zhou YS and Tiersten HF (1994) An elastic analysis of laminated composite plates in cylindrical bending due to piezoelectric actuators. *Smart Materials and Structures* 3(3): 255.